RESEARCH ARTICLE

Contrasting Impact of Future CO_2 Emission Scenarios on the Extent of $CaCO_3$ Mineral Undersaturation in the Humboldt Current System

A. C. Franco[1] (iD), N. Gruber[1] (iD), T. L. Frölicher[1,2,3] (iD), and L. Kropuenske Artman[1]

[1]Environmental Physics, Institute of Biogeochemistry and Pollutant Dynamics, ETH Zürich, Zürich, Switzerland, [2]Climate and Environmental Physics, Physics Institute, University of Bern, Bern, Switzerland, [3]Oeschger Centre for Climate Change Research, University of Bern, Bern, Switzerland

Abstract The eastern boundary upwelling systems are among those regions that are most vulnerable to an ocean acidification-induced transition toward undersaturated conditions with respect to mineral $CaCO_3$, but no assessment exists yet for the Humboldt Current System. Here we use a high-resolution (∼7.5 km) regional ocean model to investigate past and future changes in ocean pH and $CaCO_3$ saturation state in this system. We find that within the next few decades, the nearshore waters off Peru are projected to become corrosive year round with regard to aragonite, the more soluble form of $CaCO_3$. The volume of aragonite undersaturated water off Peru will continue to increase in the future irrespective of the amount of CO_2 emitted to the atmosphere. In contrast, the development of the saturation state with regard to calcite, a less soluble form of carbonate, depends strongly on the scenario followed. By 2050, calcite undersaturation appears in the nearshore waters off Peru occasionally, but by 2090 in a high-emission scenario (RCP8.5), ∼60% of the water in the euphotic zone will become permanently calcite undersaturated. Most of this calcite undersaturation off Peru can likely be avoided if a low emission scenario (RCP2.6) consistent with the Paris Agreement is followed. The progression of ocean acidification off Chile follows a similar pattern, except that the saturation states are overall higher. But also here, calcite undersaturated waters will become common in the subsurface waters under the RCP8.5 scenario by the end of this century, while this can be avoided under the RCP2.6 scenario.

Plain Language Summary The oceanic uptake of anthropogenic carbon dioxide represents a large ecosystem service to humanity, but it leads to ocean acidification, which can stress marine life in a major manner. Here we show that as a result of ocean acidification, the nearshore waters of the Humboldt Current System are bound to become undersaturated with respect to the carbonate mineral aragonite within the next decades. In contrast, future calcite undersaturation depends strongly on future carbon emissions. In a high emission scenario, year round-calcite undersaturation will develop by the end of the century. In contrast, if an emission scenario consistent with the Paris agreement was followed, the development of calcite undersaturation can be largely avoided, saving marine ecosystems from a major threat.

1. Introduction

Eastern boundary upwelling systems (EBUS) belong to the most productive ecosystems of the world's ocean (Fréon et al., 2009). The EBUS account for about 11% of global new production (Chavez & Toggweiler, 1995) and up to 20% of the global fish catch (Pauly & Christensen, 1995), even though they cover only ∼1% of the global surface ocean area. This high productivity is a consequence of equatorward wind leading to the upwelling of nutrient rich waters that fuel the strong phytoplankton growth and supports some of the world's most diverse marine ecosystems (Fréon et al., 2009). The upwelling also brings waters with high dissolved inorganic carbon, low pH, and low saturation states with respect to $CaCO_3$ to the surface (Feely et al., 2008; Hauri et al., 2009). This makes these regions sources of CO_2 to the atmosphere, and together with the Southern Ocean (Orr et al., 2005) and the Arctic Ocean (Qi et al., 2017; Steinacher et al., 2009), particularly susceptible to the effects of ocean acidification (Gruber, 2011). This is especially the case for the Pacific EBUS, namely the California and Humboldt Current Systems (HumCS), as these systems naturally have

already among the lowest pH and $CaCO_3$ saturation levels (Chavez et al., 2008; Hauri et al., 2009, 2013; Mayol et al., 2012). Currently, more than 99% of the upper global ocean is supersaturated with regard to $CaCO_3$ (Jiang et al., 2015) but model simulations have shown that an unabated continuation of ocean acidification by the oceanic uptake of anthropogenic CO_2 can push the EBUS quickly into unchartered territory, and particularly into conditions where the upper waters become corrosive with regard to mineral $CaCO_3$ (Gruber et al., 2012).

The $CaCO_3$ saturation state of seawater is commonly quantified by Ω, defined (in very good approximation) as the ratio of the in situ carbonate ion concentration over the saturation concentration of the carbonate ion with respect to mineral $CaCO_3$ (Zeebe & Wolf-Gladrow, 2001), with $\Omega > 1$ indicating supersaturation, and $\Omega < 1$ indicating undersaturation. Most marine calcifiers, including animals such as corals, bivalves, pteropods, and foraminifera, but also plants such as coralline algae and coccolithophores (Milliman, 1993), tend to react quite sensitively to changes in Ω, irrespective of whether they form their structures out of the more soluble form of $CaCO_3$, i.e., aragonite, or the more stable form, calcite (Doney et al., 2009; Kroeker et al., 2013; Pörtner et al., 2014). The response to changes in Ω is highly species specific (Doney et al., 2009; Fabry et al., 2008) or even morphotype dependent (Iglesias-Rodriguez et al., 2008), with many organisms showing clear negative responses already at rather high saturation levels (Barton et al., 2012; Byrne et al., 2013; Fabry et al., 2008). But across all taxa, the saturation threshold of $\Omega = 1$ provides a clear limit beyond which corrosion is thermodynamically favored, leading in nearly all studied organisms to dissolution effects (Bednaršek et al., 2012; Fabry et al., 2008). Even in those organisms that might be able to protect their $CaCO_3$ structures from the corrosive environment or that have mechanisms to repair the damages impaired by dissolution, the exposure to such low saturation states comes with a cost that reduces their environmental fitness (Fabry et al., 2008; Maas et al., 2012; Mackey et al., 2015).

While a substantial amount of work has addressed ocean acidification in the California Current System (Feely et al., 2008; Gruber et al., 2012; Harris et al., 2013; Hauri et al., 2009; Turi et al., 2016), very little is known about the current state and future progression of ocean acidification in the HumCS, located off the west coast of South America, straddling Peru and Chile. The strong upwelling make this EBUS the most productive of the EBUS (Carr, 2002; Lachkar & Gruber, 2012), but also leads to high values of surface pCO_2 and low values of Ω (Friederich et al., 2008; Mayol et al., 2012). Here we investigate the past, present, and future evolution of ocean acidification in the near-surface waters of the HumCS using a high-resolution regional ocean circulation model with an embedded ocean biogeochemical module. We focus on the progression of the saturation state of seawater with regard to $CaCO_3$ in the nearshore waters under two contrasting emission scenarios, the "business as usual" scenario RCP8.5 and the "strong mitigation" scenario RCP2.6. The latter leads to a global warming that is roughly consistent with the 2°C target of the Paris Agreement, while the former is expected to lead to a global warming in excess of 4°C by 2090 and more beyond the end of this century (Collins et al., 2013).

We investigate here only the effect of rising atmospheric CO_2, not considering the additional changes that might occur owing to changes in climate or any other anthropogenic perturbation. This focus is motivated by many studies having shown that for pH and other parameters of the inorganic carbon system in the near-surface ocean, the trend signals imparted by the uptake of anthropogenic CO_2 from the atmosphere will exceed those driven by climate variability and change within a few decades (Frölicher et al., 2016; Lovenduski et al., 2016; Orr et al., 2005; Steinacher et al., 2009). This is not only the case for the surface ocean where changes in ocean acidification tend to be closely tied to the changes in atmospheric CO_2 (Sarmiento & Gruber, 2006), but also at depth, where theoretically, climate change could be more important. For example, using a suite of Earth System Models, Resplandy et al. (2013) explicitly highlight for mode and intermediate waters that "physical and biological climate change feedbacks explain less than 10% of the simulated changes." Thus, by the end of the 21st century, the most important source of uncertainty with regard to the future evolution of OA appears to be the uncertainty associated with the atmospheric CO_2 scenario and not that associated with climate change and internal variability.

2. Materials and Methods

2.1. Model Description and Simulations

The physical model is the Regional Ocean Modeling System (ROMS; Marchesiello et al., 2003; Shchepetkin & McWilliams, 2005) configured for the South American West Coast. We used a spherical grid with a horizontal resolution of 7.5 km covering the region from 15°N to 40°S and from 70°W to 100°W. In the vertical, the

model resolves 32 terrain-following levels with higher resolution near the surface. For the biogeochemical module, we employed a nitrogen based NPZD (Nitrate-Phytoplankton-Zooplankton-Detritus) model (Gruber et al., 2006) extended with a carbon and oxygen module (Hauri et al., 2013).

In total, we conducted six time-slice simulations consisting of (i) a preindustrial simulation representing conditions for year 1870, (ii) a "present-day" simulation representing year 2000, (iii) two simulations for the year 2050 under RCP8.5 and RCP2.6 forcing, respectively, and (iv) two simulations for the year 2090 under the same two scenarios. For all simulations, the model was forced at the surface and at the lateral boundaries with the same present-day climatological conditions, with the exception being the concentration of atmospheric CO_2 and the lateral boundary condition for dissolved inorganic carbon (DIC) that varied between each of the six time-slices considered. The simulations were designed in this manner to account exclusively for the effect of oceanic uptake of anthropogenic carbon on the pH and calcium carbonate saturation state of the seawater. The carbonate system parameters were calculated offline following the standard routines from the Ocean Carbon Cycle Model Intercomparison Project (OCMIP-2; http://ocmip5.ipsl.jussieu.fr/OCMIP/). The dissociation constants used are those presented by Mehrbach et al. (1973), as refitted by Dickson and Millero (1987). All pH values shown here are on the seawater scale.

The atmospheric CO_2 for the preindustrial year (1870) and for year 2000 was prescribed to 286 and 370 μatm, respectively, computed from the atmospheric mixing ratios considering the mean atmospheric pressure and assuming 100% relative humidity. For the future time-slices we used a "business as usual" (RCP8.5), and a strong mitigation (RCP2.6) scenario. For 2050, the atmospheric CO_2 for the two scenarios are 538 μatm (RCP8.5) and 442 μatm (RCP2.6), while for 2090, those concentrations are 841 and 428 μatm, respectively. The lateral concentration of DIC for the preindustrial and future time-slices was extracted from output of a transient simulation of the global coupled carbon-climate Earth System Model GFDL ESM2M (Dunne et al., 2012; Rodgers et al., 2015). This global Earth System Model was run transiently from year 1861 to 2100 with prescribed atmospheric pCO_2 following the same scenarios we used in our regional model (RCP8.5 and RCP2.6). We took 20 years averaged anomalies (e.g., the average of the years 2081–2100 minus the average of the years 1986–2005) and added them to the present-day DIC values from the Global Data Analysis Project (Key et al., 2004). Although the DIC in this Earth System Model simulation is affected by both changes in climate and atmospheric CO_2, we show in the supporting information section 4 on the basis of a CO_2-only simulation for RCP8.5, that the changes in DIC and implied changes in the saturation state induced by climate change correspond to approximately 10% of those driven by the change in atmospheric CO_2. Since we are lacking a corresponding CO_2-only simulation for RCP2.6, we use the CO_2 and climate simulations for both scenarios to ensure consistency.

At the surface, we forced the model with monthly climatologies of heat and freshwater fluxes obtained from the Comprehensive Ocean-Atmosphere Data Set (COADS) database (da Silva et al., 1994), while the wind stress was taken from the Scatterometer Climatology of Ocean Winds (SCOW) climatology (Risien & Chelton, 2008), applied also at a monthly resolution. The lateral boundary forcing for temperature, salinity, oxygen, and nitrate was constructed using the data from the World Ocean Atlas 2013 (Garcia et al., 2014a, 2014b; Locarnini et al., 2013; Zweng et al., 2013; supporting information Table S1). All time-slice simulations were run for 15 years, with the years 11–15 used for the analyses.

2.2. Model Evaluation

We focus here on the evaluation of the carbonate system, including surface ocean pCO_2 and ocean interior Ω_{arag} and Ω_{calc}, the latter computed from in situ measurements of DIC and total alkalinity. For the evaluation of the physical properties, we refer to prior publications that employed a comparable setup of ROMS for the HumCS (Colas et al., 2008, 2012) as well as the supporting information, where we compare the modeled surface temperature and salinity against our initial conditions (WOA2013; Locarnini et al., 2013; Zweng et al., 2013) but also against the Simple Ocean Data Assimilation (SODA v1.4.2; Carton & Giese, 2008). Additionally, the vertical profiles of temperature, salinity and nitrate are compared against the observations contained in the CSIRO Atlas of Regional Seas (CARS2009) gridded data set (Ridgway et al., 2002). While we compare against surface pCO_2 observations that reflect (nearly) a climatological mean distribution, the interior data are very sparse in time and space. Thus, great care must be taken when comparing our climatologically forced simulations with such spot measurements. Nevertheless, these data are the only constraints we have to assess whether our model simulated ocean interior fields bear any resemblance to reality.
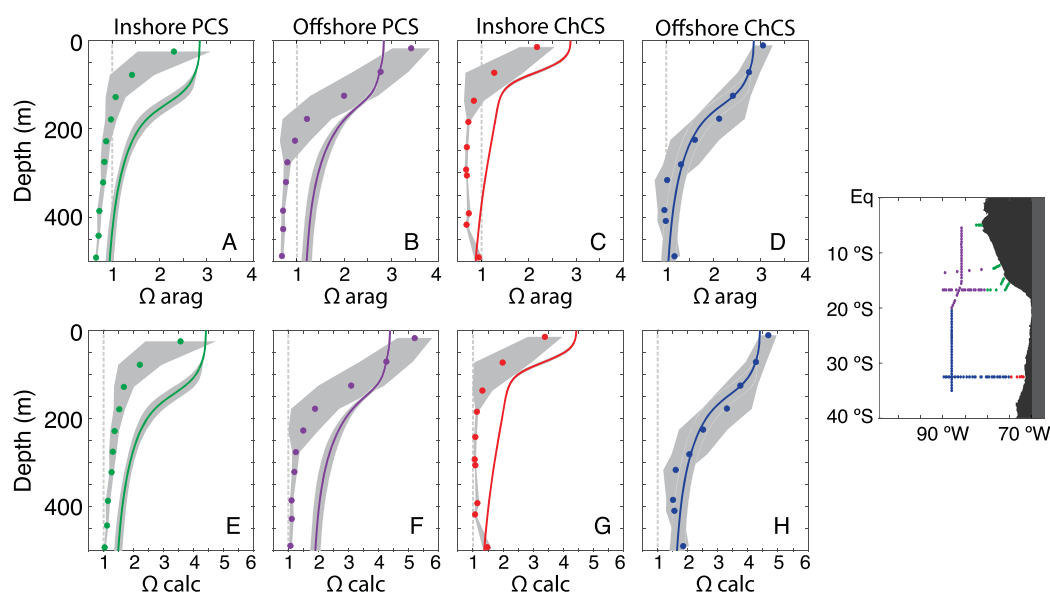
Figure 1. (a–d) Averaged vertical profiles of Ω_{arag} over different regions off the Humboldt Current System: inshore Peru (green), offshore Peru (purple), inshore Chile (red), and offshore Chile (blue). (e–h) Averaged vertical profiles of Ω_{calc} for the same regions. The solid colored lines show the model results. The dots show measured in situ values at the locations shown in the reference map. The gray areas for each profile are the standard deviations calculated at each depth of the observed and modeled averaged profiles. The dashed vertical line indicates the saturation value.

For the surface ocean pCO$_2$, we used the gridded climatology of Landschützer et al. (2014) which was interpolated from SOCAT using a neural network approach (Landschützer et al., 2013), as well as the raw data from the SOCATv4 (Bakker et al., 2016) and the LDEO (version 2012) data bases (Takahashi et al., 2013). For the ocean interior, we used the *DIC* and total alkalinity data contained in the GLODAPv2 database (Lauvset et al., 2016). From this data set, we extracted the data for the regions off Peru and Chile, respectively (Figure 1). The observations include four cruises at 5°S, 12°S, 15°S, and 16°S obtained in 1992 and 1994, respectively, two transects at 32.5°S from 2003 and 2010, and a meridional cruise obtained in 2009 extending from 5°S to 40°S. The saturation states Ω_{arag} and Ω_{calc} were computed from the measured *DIC*, alkalinity, temperature, and salinity in the same manner as done for the model. In order to remove the effect of eddies and other smaller scale variations, we averaged these data over four regions to create regional mean profiles. These regions include the nearshore regions off Peru and Chile, respectively, as well as their offshore counterparts, with the north-south boundary set at 20°S, and the offshore boundary set at about 500 km offshore. We evaluate the model by comparing the annual mean time-slice simulation representing the nominal year 2000 with the observations mentioned above, recognizing that the limited observations are potentially substantially biased by seasonal and interannual variations.

In general, the simulated saturation states (solid lines in Figure 1) agree reasonably well with the observations (dots with shaded areas in Figure 1). The model captures the overall surface to depth gradient very well, and in the offshore region of Chile, the model matches the profiles of Ω_{arag} and Ω_{calc} nearly perfectly (Figures 1d and 1h). But in the other regions (Figures 1a–1c and 1e–1g), the model fails to simulate the details of the vertical gradient in the ocean's thermocline. The model tends to generally overestimate Ω and also simulates a too deep transition from the elevated high surface saturation states to the low saturation states in the ocean interior. This leads to an overestimation of the saturation horizons, i.e., the depth where Ω becomes unity, by up to 300 m. Some of the differences in the near-surface ocean could be due to seasonal biases in the observations, but the general overestimation throughout most of the upper ocean likely reflects a model bias. In fact, the places where Ω is overestimated by the model correspond also to the places where the density is underestimated (see supporting information Figure S3), indicating that the main cause of the bias is a too deep thermocline in the model.

The overall overestimation of the modeled aragonite and calcite saturation states at depth implies that our model simulated shoaling of the saturation horizons needs to be viewed as a conservative estimate, with

the implication that the transitions modeled here might actually occur earlier, at lower atmospheric pCO_2 levels. We refrain here from applying a bias correction (as done, for example by Orr et al. (2005) and Steinacher et al. (2009)), because the observations are too scarce to firmly establish the magnitude of the bias.

The comparison of the modeled surface ocean pCO_2 (which is also a relatively good proxy for pH) with the observations reveals a similar picture (see supporting information Figure S5 and supporting information Table S2). The model tends to simulate a slightly too high surface pCO_2, amounting to a positive bias of $\sim$4 μatm in the annual mean and across the whole domain (excluding the first 100 km from the coast). This overestimation corresponds to an underestimation of Ω of less than 0.05 units, i.e., smaller than the surface biases for Ω. This suggests that the surface differences seen in Figure 1 could indeed reflect a seasonal bias in the observations. There are not enough observations in the nearshore to construct a true climatology of pCO_2 there, but the simulated range is well within the observed range determined from the raw observations (cf., supporting information Table S2), particularly when considering that the nearshore pCO_2 observations contained in the SOCATv4 and the LDEO databases are on the low side relative to the much more abundant measurements reported by Friederich et al. (2008). Details on these calculations and further comparisons can be found in the supporting information (Echevin et al., 2008; Lee et al., 2006; Takahashi et al., 2006; Turi et al., 2014; Wang et al., 2014).

In summary, the evaluation of the simulated inorganic carbonate system with the currently available observations in the HumCS suggests that the model successfully captures the main modes of the spatial variability. Additional model evaluations in the supporting information Figures S1–S5 show that the large-scale ocean circulation and many details of the upwelling dynamics are also well captured by our model setup. We thus consider the model well suited to investigate how the changes in atmospheric CO_2 has affected the pH and the saturation states until now, and how it will affect them in the coming decades. However, we clearly will need to discuss the implications of our identified biases on the results and our conclusions.

3. Progression of Near-Surface Ocean Acidification

As the atmospheric CO_2 increases between the preindustrial ($\sim$1870), the present, and the future, the surface pH and the saturation states with respect to aragonite (Ω_{arag}) and calcite (Ω_{calc}) decrease across the entire HumCS (Figure 2). While the absolute changes are spatially relatively uniform, these changes act upon regionally very different initial (preindustrial) distributions. This leads also to a rather different regional evolution with regard to the transition toward undersaturated conditions.

For preindustrial times, the model reconstructs for the open ocean HumCS surface pH, Ω_{arag} and Ω_{calc} values that are similar to those of the low latitudes (Feely et al., 2009; Figures 2a, 2e, and 2i). But in the nearshore areas, particularly those off Peru and to a lesser degree off Chile, the values are much lower in comparison to the rest of the world's ocean present values (see also Figures 3a–3d). Off Peru, a large part of the nearshore 50 km has preindustrial pH values below 8, and Ω_{arag} and Ω_{calc} saturation levels below 2.2 and 3.4, respectively. Even more extreme is the nearshore 15 km region between 5°S and 15°S (nearshore box in Figure 3a), where the preindustrial annual mean surface pH was simulated to be as low as 7.89 $\pm$ 0.04 (1 SD of the spatial mean), which is $\sim$0.3 pH units lower than the preindustrial global average surface pH (Feely et al., 2009). Such low values are also a condition that the global surface ocean will only experience in the second half of this century and only if a high-emission scenario is followed (Bopp et al., 2013; Gattuso et al., 2015). Similarly, low values in relation to global average conditions are reconstructed in this nearshore region for Ω_{arag} (Figures 3a and 3b) and Ω_{calc} (Figures 3c and 3d). Although these values are well above saturation (1.94 $\pm$ 0.22 for Ω_{arag} and 3.01 $\pm$ 0.33 for Ω_{calc}), the annual mean values are approximately 1–1.5 units below the present-day global ocean mean (Jiang et al., 2015).

Off Peru, even lower saturation states are modeled to occur in winter (JJA: June–July–August), also extending substantially further offshore than in summer (DJF: December–January–February; Figures 3e–3h). The largest seasonal amplitude is found in the region between 50 and 200 km offshore, reflecting the winter entrainment of very low saturation waters during the deepening of the mixed layer. The seasonal variations are much smaller in the very near shore region, largely owing to the compensatory nature on the saturation states between variations in upwelling and productivity. Further offshore, beyond about 500 km from the Peruvian shore, the seasonal variations are relatively small.
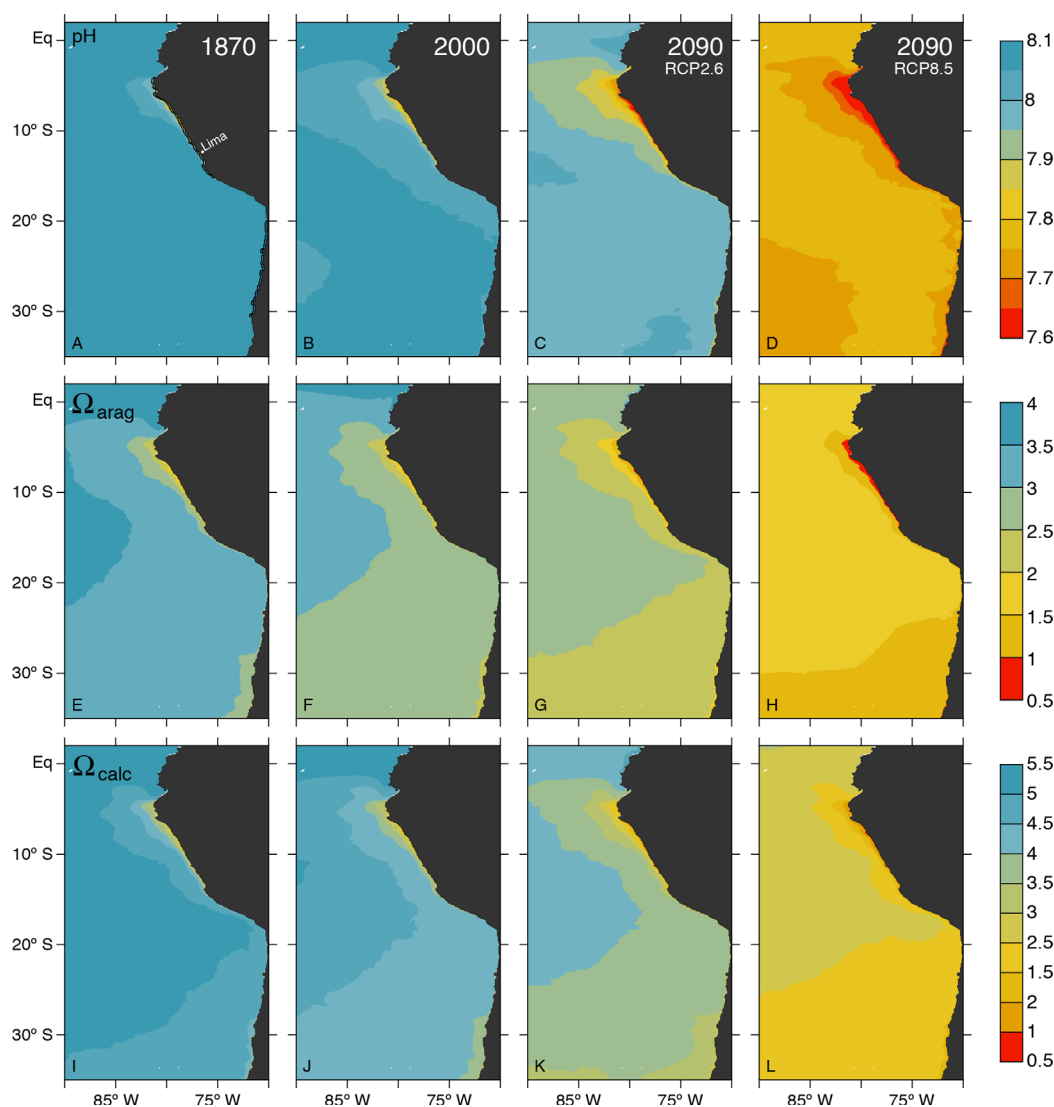
Figure 2. Evolution of surface ocean acidification in the Humboldt Current System. (first row) Annual mean surface pH for the (a) preindustrial (1870), (b) 2000, (c) 2090 (RCP2.6), and (d) 2090 (RCP8.5) time-slices. (second row) As for the first one, but (e–h) for the annual mean surface saturation state with respect to aragonite (Ω_{arag}). (third row) As for the first one, but (i–l) for the annual mean surface saturation state with respect to calcite (Ω_{calc}).

In contrast to the situation off Peru, the mean values as well as the offshore-onshore gradient of the carbonate chemistry are less pronounced off the coast of Chile (Figure 4). Despite this, the waters in the nearshore 15 km are simulated for the year 2000 to have an annual mean Ω_{arag} of 2.44 ± 0.16 and an annual mean Ω_{calc} of 3.78 ± 0.23, that is still lower than the global mean (Jiang et al., 2015). As is the case for the Peruvian sector of the HumCS, the lowest saturation states occur in austral winter (JJA) when upwelling is strongest.

This low starting point in all the parameters of the carbonate chemistry in the coastal surface waters off Peru and Chile imply a potential for an early and rapid transition toward widespread undersaturated conditions with regard to mineral $CaCO_3$. By the year 2000, the surface pH in the HumCS dropped by about ~0.1 units, while Ω_{arag} and Ω_{calc} dropped by 0.2 and 0.4 units, respectively, relative to preindustrial conditions (Figures 2b, 2f, and 2j). These changes correspond to the global trend (Bopp et al., 2013; Feely et al., 2009; Steinacher et al., 2009), indicating that like most of the global ocean, also the surface carbonate system in the HumCS has closely followed the atmospheric CO_2 perturbation. This does not lead yet to the appearance of undersaturation, but off Peru during the season of maximum upwelling (JJA), surface Ω_{arag} starts to approach unity (Figure 3f).
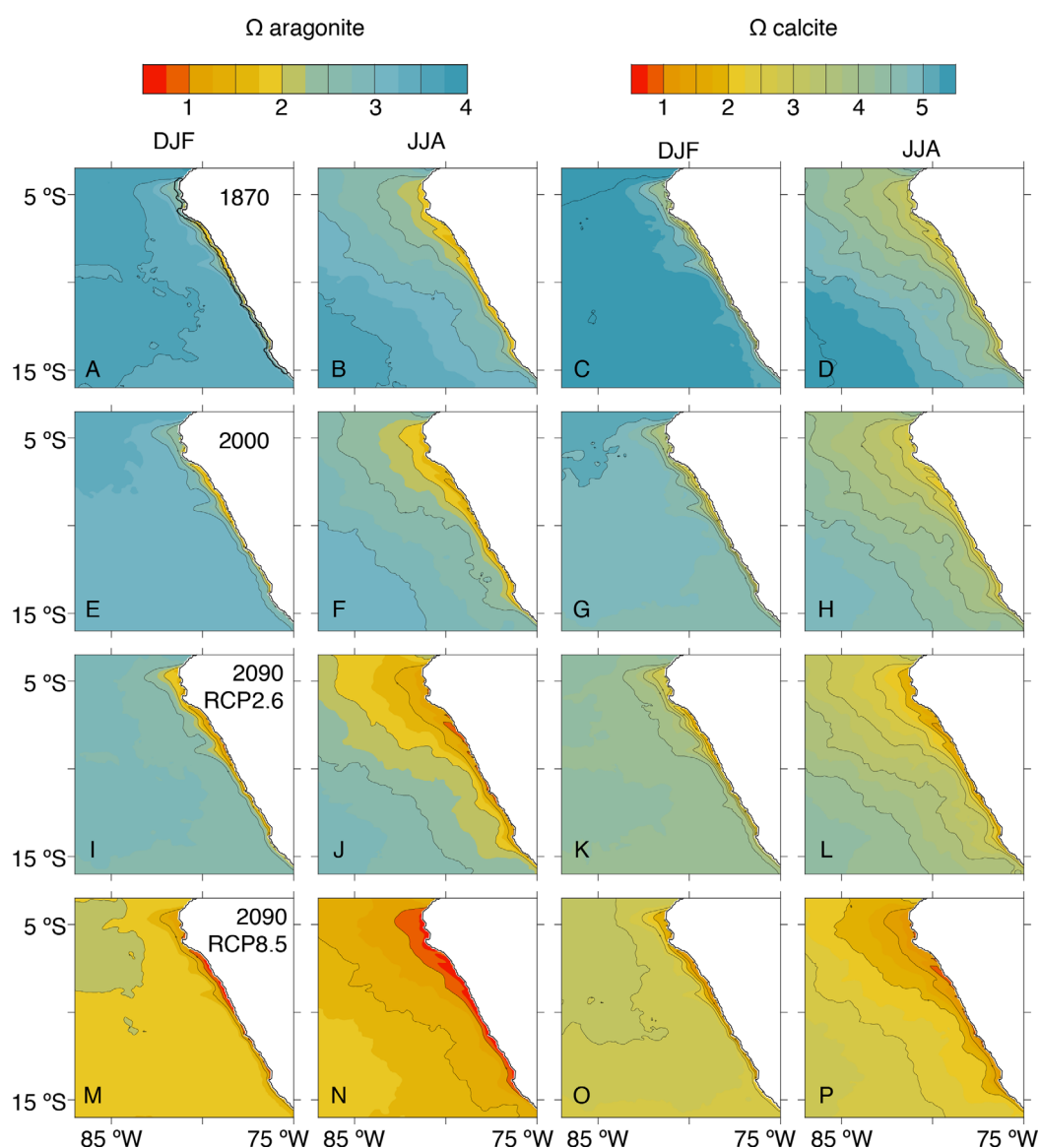
Figure 3. Evolution of surface ocean saturation states with regard to aragonite (Ω_{arag}) and calcite (Ω_{calc}) off Peru. (a–d) Conditions for preindustrial times (1870), (e–h) conditions for the year 2000, (i–l) conditions for 2090 (RCP2.6 scenario), and (m–p) conditions for 2090 (RCP8.5 scenario). (first two columns) Ω_{arag} for December–February and June–August, respectively. (third and fourth columns) As before, but for Ω_{calc}. Also shown is the boundary of the 15 km nearshore region in Figure 3a used for subsequent analyses.

If the high-emission scenario RCP8.5 was followed, the surface ocean along the entire coast off Peru will become undersaturated with regard to aragonite year long by 2090, resulting in a surface annual mean Ω_{arag} of 0.80 ± 0.14 in the nearshore 15 km band (Figure 2h). In winter (JJA), the Ω_{arag} values go as low as 0.70 in this region (Figure 3n) while they hover only slightly below 1 in summer (Figure 3m). The regions further offshore will remain supersaturated in the annual average, but a good fraction beyond the coastal 15 km band becomes undersaturated during winter (Figure 3n).

Perhaps even more concerning is the appearance of pockets of yearlong-undersaturated conditions with respect to calcite at the end of the 21st century along the coast off Peru, even though averaged over the nearshore 15 km region, the surface ocean remains slightly supersaturated (1.24 ± 0.22). During the maximum upwelling season (austral winter), a large part of the nearshore becomes undersaturated, with a regional seasonal mean Ω_{calc} of 1.09 ± 0.05 (Figure 3p). This high-emission projection contrasts strongly with the low emission scenario RCP2.6, for which the entire surface will remain supersaturated with respect
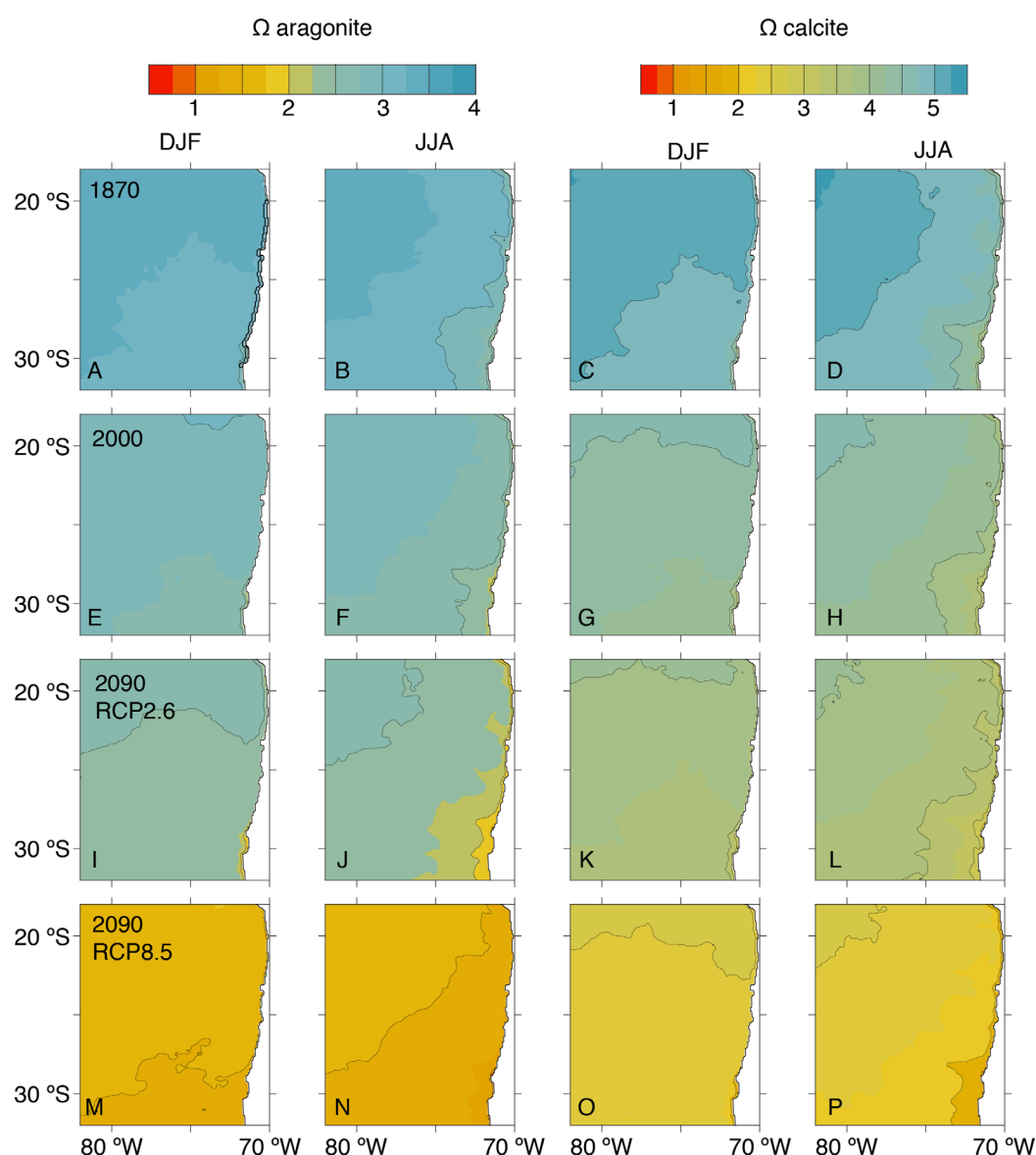
Figure 4. As Figure 3, but for the region off Chile.

to calcite (Figures 3k and 3l) and also the undersaturated conditions with respect to aragonite will be much less severe (Figures 3i and 3j).

Although the region off Chile exhibits higher annual mean surface pH and $CaCO_3$ saturation states values than off Peru, the absolute change in the $CaCO_3$ saturation states from preindustrial to the end of the century conditions is larger (regardless of the scenario followed). This larger trend off Chile is mainly due to the larger reduction of the initial concentration of carbonate ion off Chile, i.e., is a direct consequence of the nonlinearity of the carbonate chemistry (see section 4). When following the RCP8.5 scenario, surface pH within 15 km off the coast declines by nearly 0.4 units in the year 2090. Similarly, annual mean surface Ω_{arag} near the coast decreased $\sim$1.5 units to 1.29 $\pm$ 0.12 in year 2090, straddling undersaturated conditions in winter (Figure 4n), while this decrease is "only" $\sim$1.15 units in the region off Peru (Figures 2a and 2d). In contrast, if RCP2.6 is followed Ω_{arag} values remain above 2 (2.04 $\pm$ 0.16) on the annual mean. The conditions for Ω_{calc} at the end of the century are less dramatic off Chile than off Peru. Near the coast, the annual mean surface values decrease to 2.00 $\pm$ 0.18 in 2090 under high CO_2 emissions conditions, while under the RCP2.6 scenario surface Ω_{calc} near the coast remains well above saturation (3.16 $\pm$ 0.24).
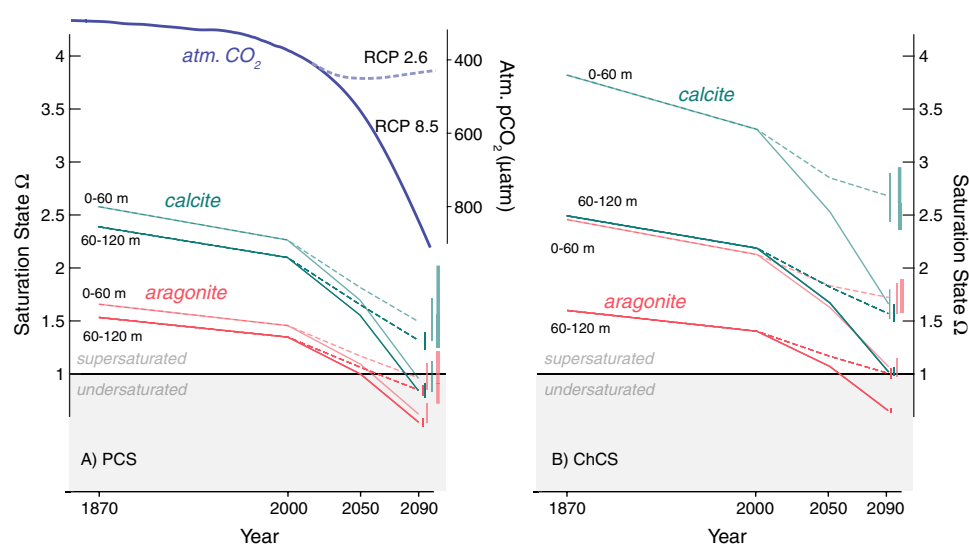
Figure 5. Temporal evolution of ocean acidification in the nearshore 15 km off the coast of (a) Peru and (b) Chile in response to different carbon emission scenarios. Shown in blue is the atmospheric CO_2 concentration (inverted, right axis), in red Ω_{arag}, and in green Ω_{calc}. The solid lines indicate the evolution for the historical period and the RCP8.5 scenario for the future. The dashed lines indicate the results for the RCP2.6 scenario. The thin vertical bars on the right hand side of each figure indicate the seasonal range of the monthly averaged values across the entire 15 km offshore band. The thick vertical lines indicate the potential variations in Ω_{arag} and Ω_{calc} induced by interannual variations associated with the El Niño-Southern Oscillation, estimated from the calculated relationship between these parameters and the observed temperature anomalies (see also section 6.1).

The striking difference between the two scenarios largely reflects the very different emission trajectories, with atmospheric CO_2 reaching a value of 840 μatm under the RCP8.5 scenario by 2090, while it increases only to 428 μatm under the RCP2.6 scenario (Figure 5a). The change in the surface ocean carbonate system tends to be "slaved" to the atmospheric CO_2 change (Gruber, 2011; Orr, 2011), owing to the rise in atmospheric CO_2 being the key driver for the oceanic uptake of anthropogenic CO_2 (or reduced outgassing of CO_2; Sarmiento & Gruber, 2006). Thus, the reduced growth of atmospheric CO_2 in the RCP2.6 mitigation scenario leads to a direct reduction in the magnitude of future ocean acidification in the surface ocean. Given rapid mixing within the upper ocean, this signal is seen throughout the upper 60 m, the layer corresponding roughly to the euphotic zone in the HumCS. Figure 5 reveals also that the separation between the two emission scenarios occurs predominantly after 2050 off Peru, with the model simulated conditions for 2050 being rather similar between the two scenarios, largely reflecting the similar atmospheric CO_2 levels at that time (Figure 5a). However, a closer inspection reveals also that in RCP2.6, ocean acidification continues to aggravate until the end of this century, even though in this scenario atmospheric CO_2 has stabilized and is actually already on a downward trend. This indicates that in this case, the progression of ocean acidification has uncoupled itself from atmospheric CO_2. In the nearshore region off Chile, the separation between the two scenarios starts already in 2050, especially in the surface layer (Figure 5b).

The evolution of ocean acidification within the upper twilight zone, i.e., the upper most layer of the aphotic zone between 60 and 120 m, follows largely that of the surface and the euphotic zone, although with an offset reflecting the lower pH and saturation levels at depth (Figure 5). For the region off Peru, this offset leads to an earlier onset of about a decade of undersaturated conditions in the 60–120 m depth layer compared to that within the top 60 m. For the region off Chile, the saturation states in the twilight zone are substantially lower than those in the upper 60 m, owing to the presence of very strong vertical gradients in all properties, including *DIC* and alkalinity. As a consequence, the progression of ocean acidification pushes this layer toward undersaturated conditions for aragonite by the end of this century, and in the case of the RCP8.5 scenario, also very close to calcite undersaturation (Figure 5b). Thus, while the upper ocean of the upwelling system off Chile likely stays supersaturated, the layer just underneath is being pushed toward widespread undersaturation in a similar manner as the system off Peru.

4. Abrupt Shoaling of the Saturation Horizons

While the progression of the surface ocean acidification parameters (pH and Ω) is rather smooth, the shoaling of the saturation horizon is found to occur rather abruptly, that is, within the coarse temporal resolution of the model it changes much faster during the second half of the century relative to before. This shoaling is relevant since it restricts the vertical extent of the habitat in the upper ocean that is characterized by supersaturated waters and is thus amenable for organisms that cannot tolerate corrosive (undersaturated) conditions.

In year 2000 and off Peru, the annual mean saturation depth for aragonite is found at around 390 m in the offshore region, shoaling to around 300 m when approaching the continental slope (Figure 6a). For calcite,
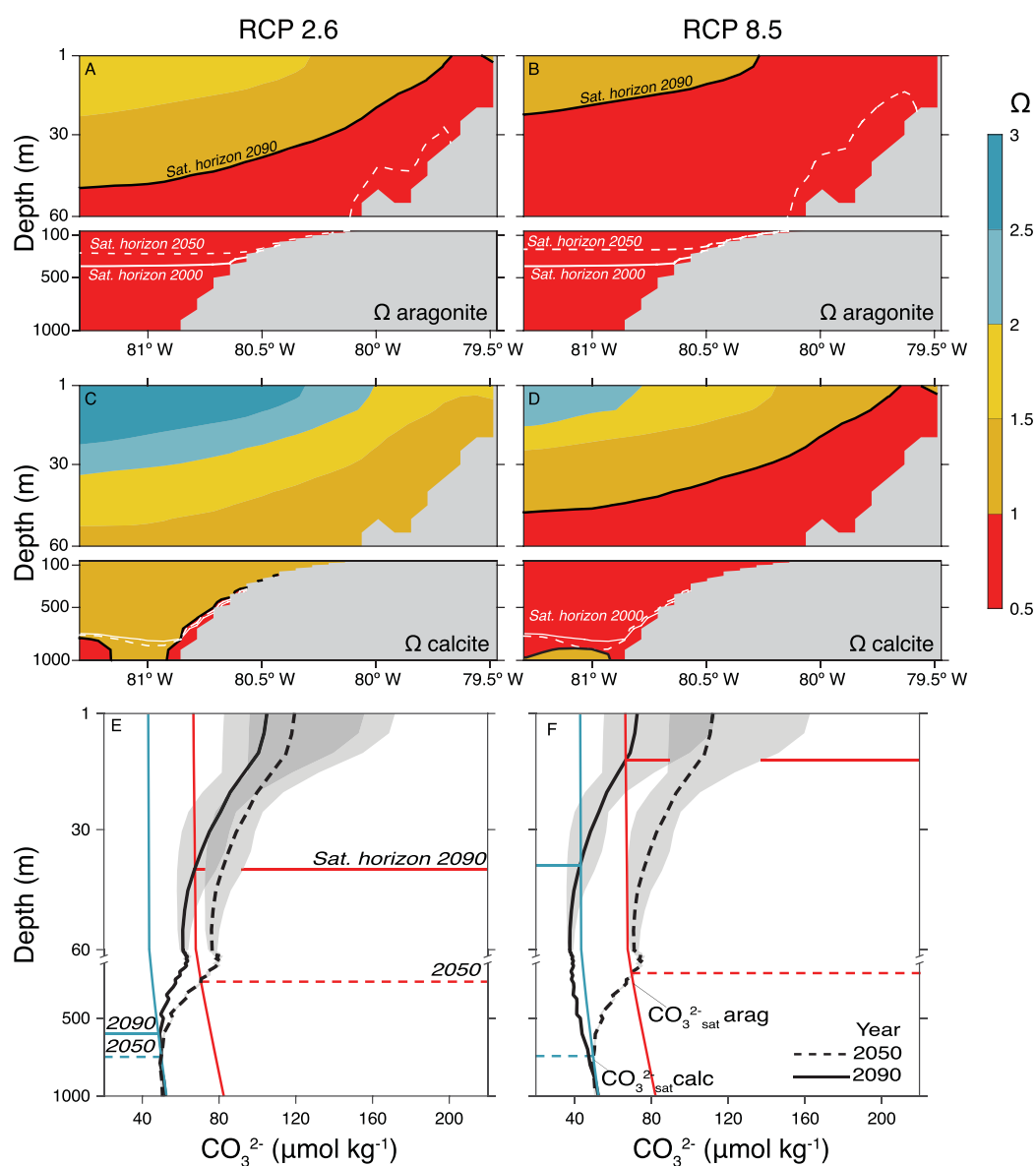

Figure 6. Progression of the vertical distribution of Ω along an offshore section at 7.5°S. (a, c, e) Conditions for year 2090 under RCP2.6. (b, d, f) Conditions for year 2090 under RCP8.5. (a, b) Ω_{arag}. (c, d) Ω_{calc}. Solid white contour: saturation horizon for year 2000; dashed white contour: saturation horizon for year 2050; solid black contour: saturation horizon for year 2090. (e, f) Vertical profiles of the carbonate ion concentration relative to the saturation concentration with respect to aragonite (red) and calcite (blue). The line in the profile is the average across the entire section shown in the other figures, and the shaded area comprises the maximum and minimum carbonate ion concentration at each depth for each time-slice. Note the break in the vertical axis at 60 m.

the saturation depth is even deeper, around 800 m, shoaling to about 500 m along the slope (Figure 6c). These depths changed little between preindustrial times and year 2000, with the total shoaling amounting to a few tens of meters (supporting information Figures S6A and S6B). But much larger changes are projected for the future. By the year 2050, and essentially independent of the emission scenario, the aragonite saturation depth is simulated to shoal by more than 150 m to ∼230 m in the offshore region and even more in the nearshore 15 km (Figures 6a and 6b). In the year 2050, aragonite undersaturated waters are found overlying almost all sediments at depths of 20 m or less, with the saturation horizon shoaling to as little as 10 m during the summer season (DJF and MAM; not shown).

The shoaling trend continues until the end of the century. In the case of the RCP8.5 scenario, the saturation depth for aragonite is projected to shoal by another 200 m to an annual average depth of 25 m in the offshore region, while closer to shore, aragonite undersaturated waters now comprise the whole water column in the first 75 km (Figure 6b). In the low emissions scenario, the situation is only slightly less severe. The aragonite undersaturated conditions across the whole water column extend only out to 20 km from the coast on the annual mean, and the aragonite saturation depth remains somewhat deeper (50 m) in the offshore region (Figure 6a). Thus, the rate of shoaling of the saturation horizon is not at all proportional to the rise in atmospheric CO_2 and the oceanic uptake of anthropogenic CO_2, as is (largely) the case for the change in pH and Ω.

This nonlinear response of the shoaling of the saturation horizon to the oceanic uptake of anthropogenic CO_2 is also seen for the calcite saturation horizon. Off Peru, this horizon shoals very little between 2000 and 2050 and remains below 700 m (Figures 6c and 6d). After 2050, large changes are potentially in store, but in contrast to Ω_{arag}, the shoaling of the calcite saturation horizon by 2090 will depend in great measure on the emission scenario. Under the RCP8.5 scenario (Figure 6d), this saturation horizon shoals right into the surface ocean, making the whole water column in the first 20 km from the coast undersaturated with respect to calcite in the annual mean. During the upwelling season, this undersaturated water column can extend as far as 50 km offshore. In the region further offshore, the calcite saturation depth is projected to shoal to 50 m depth. In contrast, the calcite saturation depth is projected to remain below 500 m by the end of the century under the RCP2.6 scenario (Figure 6c), even though the upper ocean Ω_{calc} will decrease considerably. Although this value is projected to go as low as 1.5 in the layer overlying the sediments in the top 60 m, no calcite undersaturation occurs in the top 60 m in this scenario (see also supporting information Figures S8 and S9).

The nonlinear and rather abrupt nature of the shoaling of the saturation depths can be explained in terms of the changes in the in situ carbonate ion concentration ($[CO_3^{2-}]$) relative to the concentration profile of the carbonate ion at saturation, as it is the intercept of these curves that defines the saturation horizon (Figures 6e and 6f; Hauri et al., 2013). In preindustrial times, the in situ $[CO_3^{2-}]$ profile intercepts the saturation $[CO_3^{2-}]$ profiles for aragonite and calcite at ∼350 m and ∼750 m, respectively. As anthropogenic CO_2 invades the ocean from the surface, it first titrates away the CO_3^{2-} in the upper ocean, leading to a strong reduction in the in situ $[CO_3^{2-}]$ concentration there between preindustrial times and the present. However, this has little implication for the depths of the saturation horizons, as they are beyond the reach of the present-day anthropogenic CO_2 invasion (Sabine et al., 2004). As the concentration of anthropogenic CO_2 builds up in the ocean and penetrates deeper, the $[CO_3^{2-}]$ drops also in the deeper ocean, leading to a sudden onset of the shoaling of the saturation depth. The rate of shoaling depends on the rate at which anthropogenic CO_2 is accumulating, but even more critically also on the shape of the $[CO_3^{2-}]$ profile. Wherever the vertical gradient of $[CO_3^{2-}]$ is small, the saturation depth tends to shoal quickly, because a small decrease in the $[CO_3^{2-}]$ leads to a rapid change in the aragonite saturation depth. Conversely, wherever the vertical gradient of the $[CO_3^{2-}]$ is large, the saturation depth tends to shoal slowly. This explains why the saturation horizon for aragonite shoals only slowly first, as the in situ $[CO_3^{2-}]$ gradient near the intercept with the saturation $[CO_3^{2-}]$, i.e., at ∼400 m is large during both 1870 and 2000, but this gradient is much smaller when the intercept shoals to the euphotic zone between 2050 and 2090, leading to a strong jump in the saturation horizon between these two time-slices.

While fundamentally similar, the situation is less extreme off the coast of Chile. When analyzing a similar transect perpendicular to the coast at 25°S (supporting information Figure S9), the aragonite saturation horizon shoals considerably between the different time-slices from ∼500 m in 1870 to ∼30 m near the coast by 2090 in the RCP8.5 scenario. However, contrary to the region off Peru, the aragonite undersaturated water

does not reach the surface by the end of the century (supporting information Figure S8A). This is due to the fact that the initial $[CO_3^{2-}]$ is much higher than the one off Peru (>170 μmol kg^{-1} in 2000) and although the waters below 30 m, and especially those overlying the sediments will become undersaturated by 2090 in the case of the high-emission scenario, the system will tolerate a larger increase in atmospheric CO_2 before the water column becomes completely undersaturated.

5. Habitat Restriction

The potential ecosystem implications of the development of pervasive upper ocean aragonite and calcite undersaturation conditions are manifold, particularly when considering that many calcifying organisms begin to experience stress when seawater conditions are still well above the saturation threshold (at Ω above 1; e.g., Barton et al., 2012; Byrne et al., 2013; Fabry et al., 2008). In order to determine the changes in habitat size for organisms with a particular sensitivity, we analyze the volume of water within a certain range of aragonite and calcite saturation values. We focus on the nearshore region extending 15 km off the coast of Peru (Figure 7) and off the coast of Chile (Figure 8).

The changes in habitat suitability are very large in the 15 km region off Peru (Figure 7). While only ~20% of the waters in the top 60 m had annual mean values of Ω_{arag} lower than 1.5 during preindustrial times (yellow bars), this volume increased to 60% by 2000. In addition, waters with Ω_{arag} larger than 2 (blue bars) that occurred in about 10% of the top 60 m during preindustrial times are now essentially absent (4% annual mean). By 2000, no undersaturated conditions are simulated for the upper 60 m yet, but this is bound to change. By the year 2050, and irrespective of the emission scenario, between 10% (RCP2.6) and 25% (RCP8.5) of the top 60 m of the water column will become undersaturated with respect to aragonite in the
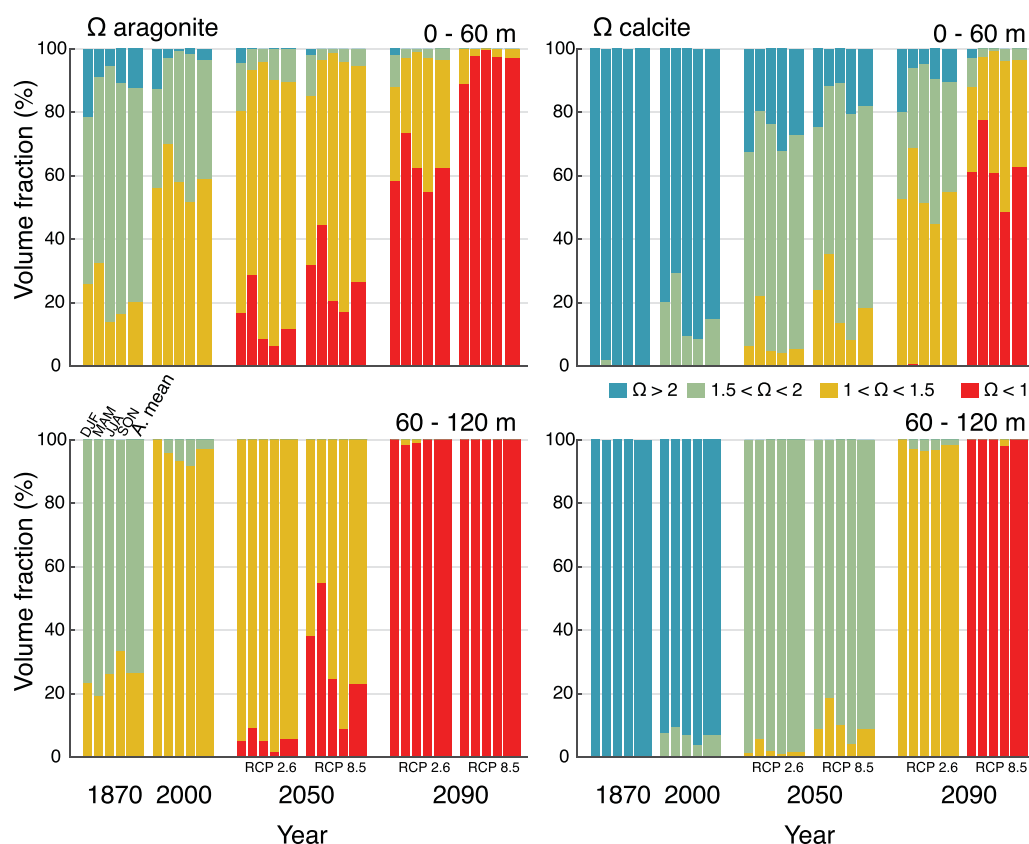

Figure 7. Volume fractions of classes of (left) Ω_{arag} and (right) Ω_{calc} within 15 km off the coast of Peru (top) for the top 60 m and (bottom) from 60 m to 120 m. Included are the simulation results for 1870, 2000, and the projections for the years 2050 and 2090 under the RCP8.5 and RCP2.6 scenario, respectively. The first four columns within each bin represent the four seasons (DJF, MAM, JJA, and SON), while the fifth represents the annual mean.
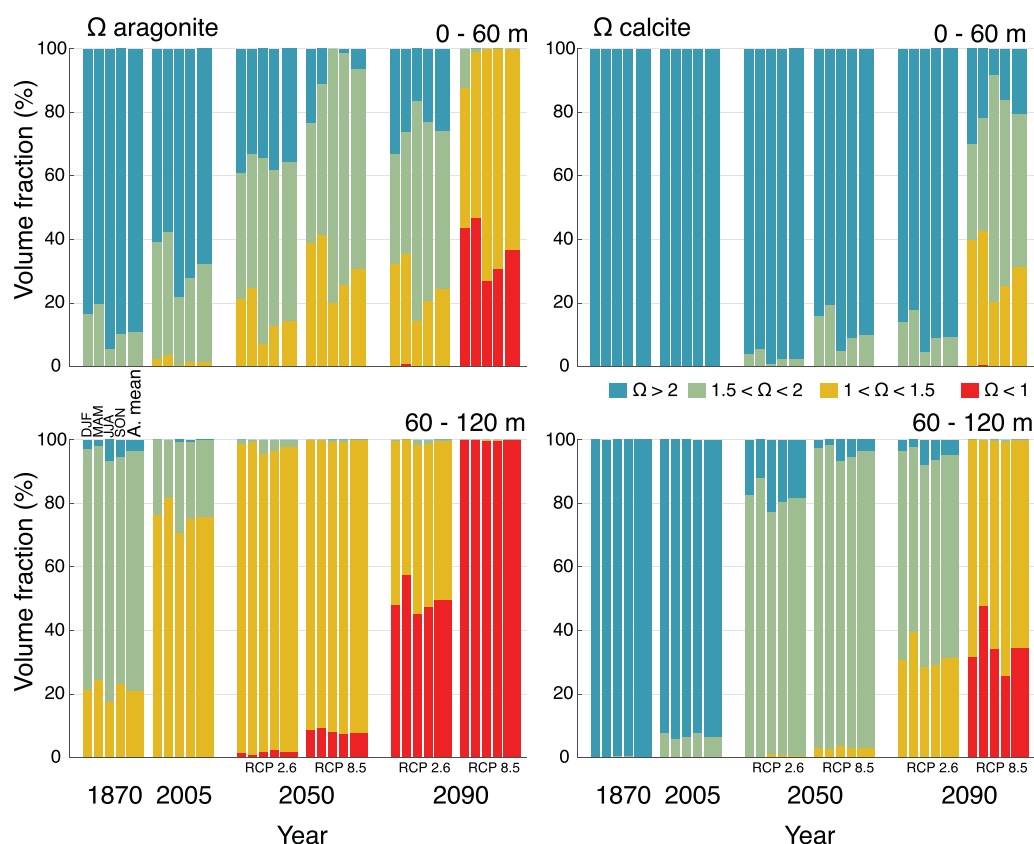
Figure 8. As Figure 7, except for the 15 km region off the coast of Chile.

annual average (red bars), with seasonal intrusions of aragonite undersaturated water doubling that fraction.

The volume of undersaturated waters continues to increase rapidly, such that by the year 2090, supersaturated waters essentially have vanished from the top 60 m of the water column under the RCP8.5 scenario, leaving no habitat for organisms that are sensitive to corrosive conditions with respect to aragonite. Under the RCP2.6 scenario, however, 40% will remain supersaturated, primarily in the very near surface and during the spring-summer (SON-DJF) season, when strong photosynthetic activity can reduce the surface ocean CO_2 concentration, thereby raising pH and the saturation state.

The subsurface layer (60–120 m) saturation levels progress in a similar manner as the top 60 m, but with an earlier transition toward widespread undersaturation. The fraction of waters undersaturated with respect to aragonite is simulated to increase rapidly from being absent in year 2000 to 5 to 25% in 2050 and then to 100% in 2090, with only a small difference between the two scenarios considered. The rapid transition from about 5% undersaturated conditions in 2050 to 100% undersaturated conditions in 2090 is particularly striking for the RCP2.6 scenario, since atmospheric CO_2 actually decreases during this period in this scenario (Figure 5a).

In the case of the saturation state with respect to calcite, the fraction of water with values greater than two (blue bars in Figure 7) in the top 60 m within 15 km off the coast of Peru has already decreased from occupying the totality of the water column in preindustrial time to 85% (annual mean) in the present day. This fraction will continue to decrease to less than 25% by 2050 and waters with Ω_{calc} values between 1 and 1.5 will appear in 5% (RCP2.6) to 20% (RCP8.5) of the top layer. But by 2090, a large difference in Ω_{calc} between the two carbon emission scenarios arises. While calcite undersaturated water becomes dominant (>60%) in the top 60 m in the RCP8.5 scenario, calcite undersaturated water is not projected to occur by year 2090 under the RCP2.6 scenario. A similarly striking difference is found in the twilight zone, the 60–120 m layer,

where the fraction of water with undersaturated conditions will remain absent in the RCP2.6 scenario. However, under the RCP8.5 scenario, this layer transitions drastically from supersaturated values in 2050 to 100% calcite undersaturation in 2090. Thus, in contrast to the situation with regard to aragonite saturation levels, where the development of undersaturated conditions is essentially unavoidable given the current set of plausible projections of atmospheric CO_2 levels, the development of undersaturated conditions with respect to calcite depends greatly on the emission pathway.

In the region off Chile, the amount of carbon emitted to the atmosphere in the coming decades will also determine the degree to which calcifying organisms will experience stress until the end of the century. If the high-emission scenario (RCP8.5) is followed, by 2090 the top 60 m near the coast will have Ω_{arag} values lower than 1.5 year round (Figure 8), with 35% of the water column undersaturated with respect to aragonite. However, when the mitigation scenario (RCP2.6) is followed, no aragonite undersaturated water is projected to occur in the top 60 m. In the subsurface layer (60–120 m) aragonite undersaturated water is modeled to occupy only 50% on the annual mean by year 2090 under RCP2.6, contrasting strongly with the 100% under the high-emission scenario RCP8.5. The contrast between the two scenarios is even more evident for Ω_{calc}. Unlike the region off Peru, calcite undersaturated waters do not reach the surface layer by year 2090 under RCP8.5. But they are projected to occupy about 35% of the volume in the subsurface layer. However, undersaturated conditions with regard to calcite can be completely avoided, even in the subsurface layer, if the low emissions pathway is followed.

6. Discussion

Although the present-day values of Ω_{arag} and Ω_{calc} in the nearshore 15 km off the coast of Peru are very low in comparison with the global ocean, they are comparable with those in other hotspot regions of ocean acidification, such as the Southern Ocean and the California Current System (Feely et al., 2008; Jiang et al., 2015; McNeil & Matear, 2008). Given the similar present-day values, it is entirely expected that the onset of widespread aragonite undersaturation will occur within a similar time frame as that projected for these other two regions, which is within the coming decades (Gruber et al., 2012; McNeil & Matear, 2008; Orr et al., 2005). And as was the case for these two other systems, this onset is more or less bound to occur irrespective of which carbon emission trajectory is followed. Thus, the onset of widespread undersaturation with respect to aragonite in the nearshore areas of the northern Humboldt Current System is a development that humankind has already committed to itself and can be considered as virtually unavoidable. The situation is similar, yet less severe, for the southern parts of the nearshore HumCS (off Chile). Here, this committed undersaturation does not extend to the surface, but exists in the subsurface layer between 60 and 120 m. Although we focus here on a relatively narrow 15 km strip along the coasts of these two regions, the conclusions are not very different from those resulting from the analysis of a 50 km wide band (see supporting information plots S10 and S11).

An important reason for this unavoidable trajectory is that undersaturation is projected to occur in the surface waters off Peru and in the subsurface waters off Chile even in the case of the strong mitigation scenario RCP2.6. This was unexpected. A simple interpolation of the results from the RCP8.5 experiment would have suggested for Peru that the onset of severe undersaturation, i.e., where more than 50% of the top 60 m volume becomes undersaturated year round, would not occur until atmospheric CO_2 reached a value of $\sim$640 μatm. For RCP8.5, this occurs in 2065, while atmospheric CO_2 in the RCP2.6 scenario reaches a maximum of 443 μatm, and thus always stays well below the apparently critical value of 640 μatm (Figure 5). Thus, based on the usually strong relationship between the atmospheric CO_2 and the magnitude of ocean acidification (see e.g., Gruber et al., 2012; McNeil & Matear, 2008; Orr, 2011; Steinacher et al., 2009), the upper ocean under the RCP2.6 scenario should have remained supersaturated. Yet the extent and severity of the aragonite undersaturation continued to develop for decades after 2050, when atmospheric CO_2 ceased to increase in the RCP2.6 scenario.

This decoupling in the development of upper ocean acidification from the atmospheric CO_2 forcing in the nearshore regions of the HumCS is most likely the result of ocean circulation that brings older waters toward the coastal upwelling systems. The anthropogenic CO_2 burden in these waters tend to continue to increase, even when atmospheric CO_2 stops increasing (Frölicher & Joos, 2010; Joos et al., 2011), an effect that one observes already today for bomb radiocarbon (Graven et al., 2012). This is because these waters

usually have not been in contact with the atmosphere for several years to decades, which results in them not having fully realized the total amount of anthropogenic CO_2 burden that is consistent with the current lower level of CO_2 in the atmosphere (Resplandy et al., 2013). As a result, the ocean continues to take up anthropogenic CO_2 from the atmosphere, furthering ocean acidification in coastal upwelling systems, even though the atmospheric CO_2 has stabilized. Resplandy et al. (2013) demonstrated this effect to occur in the high latitude regions as well as some of the upwelling regions, but actually found this effect to be strongest in the eastern tropical Pacific across a range of different Earth System Models. They also showed that this delay between when the maximum in atmospheric CO_2 is reached and when the minimum saturation state occurs in the upper ocean can amount to several decades, consistent with our regional model results. Further support for our interpretation stems from the simulations with the GFDL model that we used for the lateral boundary conditions. Also in the GFDL model, the delay between the peak in atmospheric CO_2 and the trough in subsurface ocean acidification amounts to several decades in the Humboldt Current System (see supporting information Figure S14).

In strong contrast to the unavoidable onset of aragonite saturation, the development of widespread calcite undersaturation by the end of the 21st century appears avoidable. With the onset of calcite undersaturation impacting a much wider array of marine organisms than the presence of "simple" aragonite undersaturation, avoiding this consequence of the emissions of CO_2 by anthropogenic activities is of great benefit for the marine organisms of the Humboldt Current System, and ultimately for the entire ecosystem. Thus, this provides an additional argument in engaging in an aggressive mitigation pathway, so that the impact of ocean acidification can be retained within limits (Gattuso et al., 2015; Steinacher et al., 2013), even though the RCP2.6 emission pathway looks increasingly outside the realm of possibilities without major employment of negative emissions technologies (Obersteiner et al., 2018).

We focused here on the onset of undersaturated conditions by using a thermodynamically well defined threshold. While this threshold is undeniably important, it is certainly not the only threshold of relevance for biological systems. Many organisms simply react to the magnitude of the change or the rate at which these changes occur, irrespective of the absolute level of the stressor. Other organisms have critical thresholds that are much higher than that chosen here, especially corals and many larvae (Barton et al., 2012; Byrne et al., 2013; Fabry et al., 2008). It is beyond the scope of our study to assess all potential other thresholds, but we note that the selection of higher thresholds would simply tend to aggravate and accelerate the transitions described here, but not fundamentally alter the main conclusion. In contrast, if the rate of change was the most important concern for organisms, then our conclusion would not hold, as the rate of change in the regions of our study are not really different from those elsewhere. However, the evidence for the rate of change being the key driver for the impact of ocean acidification is not well established, while the presence of critical thresholds has been demonstrated clearly, as summarized by Pörtner et al. (2014).

6.1. Caveats

Even though we consider these conclusions as robust, a number of important caveats needs to be discussed, such as (i) the impact of model biases, (ii) the lack of consideration of climate variability, (iii) the lack of consideration of longer-term climate change, and (iv) the use of time-slice rather than time-continuous simulations. First, the limited observations available would suggest that our modeled saturation levels are biased high rather than low. This implies that our modeled transition to undersaturated conditions occurs more likely too late rather than too early. However, the overestimation of Ω values by the model could also imply that the increase in the volume of undersaturated water in Figures 7 and 8 is somewhat larger, since the fractional change in Ω_{arag} per unit change in anthropogenic CO_2 is larger for high than for low Ω_{arag} values. But we consider this effect to be small, since it will be mostly compensated for by the fact that the total change to reach undersaturated conditions needs to be larger owing to the positive bias in our model.

The second important caveat in our study is the lack of consideration of year-to-year variability, associated e.g., with the El Niño/Southern Oscillation (ENSO) phenomenon. Given the observation of substantial physical and biological changes associated with ENSO in the HumCS (Chavez et al., 2008), ENSO quite likely will lead to strong year-to-year changes in ocean acidification, as seen for the California Current System (Turi et al., 2016). But we do not expect a major impact in terms of the centennial-scale transition toward undersaturated conditions. However, the presence of ENSO would delay the moment when the ocean

acidification-induced changes in pH and the saturation states would move outside the current envelope of variability.

In order to assess the potential impact of ENSO on our conclusions, we estimated the likely signal of ENSO on the modeled saturation states by considering the observed relationship between Ω_{arag} and Ω_{calc} with temperature in the first 120 m of the water column taken from all the available observations in the region off Peru and off Chile from GLODAPv2. The slope obtained with this linear regression was then multiplied separately by the average temperature anomaly during all El Niño months and all La Niña months for both regions to obtain the mean change in Ω_{arag} during each condition. Afterward the Ω_{arag} values obtained were scaled with the standard deviation calculated with the full time series of temperature anomalies available (1982–2017). The temperature anomalies were obtained from NOAA for the Niño 1 + 2 region (http://www.cpc.ncep.noaa.gov/data/indices/sstoi.indices). This resulted in a zero-order estimate of the El Niño related increase in Ω_{arag} for the region off Peru of 0.46 units and a La Niña related decrease of 0.28 units. The increase in Ω_{calc} is estimated to be about 0.70 during an El Niño event, and a decrease in Ω_{calc} of 0.43 during La Niña. The associated interannual standard deviations are about 1.5 times smaller. While this variability is clearly substantial, it is still much smaller than the changes that are looming ahead, confirming the conclusions of our study.

Perhaps more concerning is the third major caveat, which is the lack of consideration of climate change. This is particularly relevant since observations have revealed a long-term trend toward stronger equatorward wind, strengthening the upwelling (Sydeman et al., 2014). We expect that a trend toward stronger upwelling would tend to exacerbate the progression toward undersaturation, as was found for the California Current System in an idealized wind enhancement experiment (Lachkar, 2014). Also a possible trend toward the upwelled waters becoming older and hence containing a larger amount of remineralized organic matter leading to lower pH and saturation states (Rykaczewski & Dunne, 2010) would tend to accelerate ocean acidification in the HumCS. Thus, with respect to all discussed caveats, our projections can be considered as conservative with regard to the speed and extent of the transition toward undersaturated conditions. This is particularly the case when it comes to the assessment of the ultimate impact of the simulated changes on marine organisms and ecosystems, as we have focused here only on one of many potential stressors, i.e., ocean acidification, leaving out the other major threats, such as warming, changes in the availability of limiting resources (nutrients, food), and ocean deoxygenation (Gruber, 2011).

A further argument for our results being robust are the results of several analyses where the relative contribution to uncertainty stemming from (i) model uncertainty, (ii) scenario uncertainty, and (iii) uncertainty arising from internal variability were quantified (e.g., Frölicher et al., 2016). These studies generally found that with regard to the progression of ocean acidification, the impact of climate variability is relatively small beyond the next 30 years, especially for surface pH (Frölicher et al., 2016). Concretely, Frölicher et al. (2016) showed that by 2050, about 70% of the total uncertainty in future projections of pH at the level of large-scale marine ecosystem regions stems from uncertainties associated with scenarios, and only 30% from model uncertainties and internal variability. We suspect that similar conclusions would have been reached for the saturation state. These results pertain to the surface ocean only, and the relative roles of the uncertainties stemming from the scenarios, models and internal variability are likely somewhat different at depth. Even though we currently lack a corresponding analysis at depth, we believe that our conclusion about scenario uncertainty being the most important determinant for the future evolution of ocean acidification in the Humboldt Current System still holds, since our results depend largely on the processes in the upper few hundred meters, i.e., are still closely related to those at the surface.

The forth and final caveat is of comparatively less concern, in our opinion. Time-slice simulations are indeed somewhat tricky, as they cannot fully reproduce the temporal evolution of a simulation run in time-continuous mode. However, by keeping the spinups for each time-slice relatively short and by adjusting both the initial and boundary conditions for each time-slice, we attempted to minimize the potential errors. This is supported by our experience in the California Current System, where we had compared time-slice with time-continuous simulations and where we found little difference (Gruber et al., 2012).

7. Conclusion

The present-day low pH and $CaCO_3$ saturation state imprinted by year-round upwelling off Peru and Chile make the nearshore regions of the HumCS particularly vulnerable to future ocean acidification. Our model

simulations suggest that off Peru, year-round aragonite undersaturation in the top 60 m is unavoidable even when carbon emissions in the next decades are reduced considerably. In addition, if CO_2 emissions continue along a "business as usual" trajectory, this region of the Humboldt Current System will become one of the first regions globally that will experience calcite undersaturation. But if emissions are curtailed, and an emission trajectory is followed that is coherent with the Paris Agreement, then the development of these calcite undersaturated conditions can likely be avoided. Off Chile, similar conclusions can be drawn, but for the subsurface waters in the twilight zone (60–120 m), i.e., while undersaturated conditions are bound to become dominant in the case of aragonite, calcite undersaturation is modeled to occur only in the high-emission RCP8.5 scenario. Thus, the different emission trajectories offer two strongly contrasting futures with regard to the development of ocean acidification in the Humboldt Current System.

References

Bakker, D. C. E., Pfeil, B., Landa, C. S., Metzl, N., O'Brien, K. M., Olsen, A., et al. (2016). Surface Ocean CO_2 Atlas (SOCAT) V3, doi:10.1594/PAN-GAEA.849770, supplement to: Bakker, DCE et al. (2016): A multi-decade record of high-quality fCO_2 data in version 3 of the Surface Ocean CO_2 Atlas (SOCAT). *Earth System Science Data*, 8(2), 383–413. https://doi.org/10.5194/essd-8-383-2016

Barton, A., Hales, B., Waldbusser, G. G., Langdon, C., & Feely, R. A. (2012). The Pacific oyster, Crassostrea gigas, shows negative correlation to naturally elevated carbon dioxide levels: Implications for near-term ocean acidification effects. *Limnology and Oceanography*, 57(3), 698–710. https://doi.org/10.4319/lo.2012.57.3.0698

Bednaršek, N., Tarling, G. A., Bakker, D. C. E., Fielding, S., Jones, E. M., Venables, H. J., et al. (2012). Extensive dissolution of live pteropods in the Southern Ocean. *Nature Geoscience*, 5(12), 881–885. https://doi.org/10.1038/ngeo1635

Bopp, L., Resplandy, L., Orr, J. C., Doney, S. C., Dunne, J. P., Gehlen, M., et al. (2013). Multiple stressors of ocean ecosystems in the 21st century: Projections with CMIP5 models. *Biogeosciences*, 10(10), 6225–6245. https://doi.org/10.5194/bg-10-6225-2013

Byrne, M., Lamare, M., Winter, D., Dworjanyn, S. A., & Uthicke, S. (2013). The stunting effect of a high CO_2 ocean on calcification and development in sea urchin larvae, a synthesis from the tropics to the poles. *Philosophical Transactions of the Royal Society B*, 368(1627), 1–13. https://doi.org/10.1098/rstb.2012.0439

Carr, M.-E. (2002). Estimation of potential productivity in eastern boundary currents using remote sensing. *Deep Sea Research Part II: Topical Studies in Oceanography*, 49, 59–80.

Carton, J. A., & Giese, B. S. (2008). A reanalysis of ocean climate using Simple Ocean Data Assimilation (SODA). *Monthly Weather Review*, 136, 2999–3017. https://doi.org/10.1175/2007MWR1978.1

Chavez, F. P., Bertrand, A., Guevara-Carrasco, R., Soler, P., & Csirke, J. (2008). The northern Humboldt Current System: Brief history, present status and a view towards the future. *Progress in Oceanography*, 79(2–4), 95–105. https://doi.org/10.1016/j.pocean.2008.10.012

Chavez, F. P., & Toggweiler, J. R. (1995). Physical estimates of global new production: The upwelling contribution. In C. P. Summerhayes et al. (Eds.), *Upwelling in the ocean: Modern processes and ancient records* (pp. 313–320). New York, NY: John Wiley.

Colas, F., Capet, X., McWilliams, J., & Shchepetkin, A. (2008). 1997–1998 El Niño off Peru: A numerical study. *Progress in Oceanography*, 79(2–4), 138–155. https://doi.org/10.1016/j.pocean.2008.10.015

Colas, F., McWilliams, J. C., Capet, X., & Kurian, J. (2012). Heat balance and eddies in the Peru-Chile Current System. *Climate Dynamics*, 39(1), 509–529. https://doi.org/10.1007/s00382-011-1170-6

Collins, M., Knutti, R., Arblaster, J., Dufresne, J.-L., Fichefet, T., Friedlingstein, P., et al. (2013). Long-term climate change: Projections, commitments and irreversibility. In *Climate change 2013: The physical science basis. Contribution of Working Group I to the fifth assessment report of the Intergovernmental Panel on Climate Change*. Cambridge, UK: Cambridge University Press. https://doi.org/10.1017/CBO9781107415324.024

da Silva, A. M., Young, C. C., & Levitus, S. (1994). *Atlas of surface marine data 1994. Volume 1: Algorithms and procedures* (Tech. Rep. NOAA Atlas NESDIS 6). Washington, DC: National Oceanic and Atmospheric Administration.

Dickson, A. G., & Millero, F. J. (1987). A comparison of the equilibrium constants for the dissociation of carbonic acid in seawater media. *Deep Sea Research Part A. Oceanographic Research Papers*, 34(10), 1733–1743.

Doney, S. C., Fabry, V. J., Feely, R. A., & Kleypas, J. A. (2009). Ocean acidification: The other CO_2 problem. *Annual Review of Marine Science*, 1, 169–192. https://doi.org/10.1146/annurev.marine.010908.163834

Dunne, J. P., John, J. G., Adcroft, A. J., Griffies, S. M., Hallberg, R. W., Shevliakova, E., et al. (2012). GFDL's ESM2 global coupled climate-carbon Earth system models. Part I: Physical formulation and baseline simulation characteristics. *Journal of Climate*, 25, 6646–6665. https://doi.org/10.1175/JCLI-D-11-00560.1

Echevin, V., Aumont, O., Ledesma, J., & Flores, G. (2008). The seasonal cycle of surface chlorophyll in the Peruvian upwelling system: A modelling study. *Progress in Oceanography*, 79(2–4), 167–176. https://doi.org/10.1016/j.pocean.2008.10.026

Fabry, V. J., Seibel, B. A., Feely, R. A., & Orr, J. C. (2008). Impacts of ocean acidification on marine fauna and ecosystem processes. *ICES Journal of Marine Science*, 65, 414–432. https://doi.org/10.1093/icesjms/fsn048

Feely, R. A., Doney, S. C., & Cooley, S. C. (2009). Ocean acidification: Present conditions and future changes in a high-CO_2 world. *Oceanography*, 22(4), 36–47.

Feely, R. A., Sabine, C. L., Hernandez-Ayon, M., Ianson, D., & Hales, B. (2008). Evidence for upwelling of corrosive "acidified" water onto the continental shelf. *Science*, 320, 1490–1492. https://doi.org/10.1126/science.1155676

Fréon, P., Barange, M., & Aristegui, J. (2009). Eastern boundary upwelling ecosystems: Integrative and comparative approaches. *Progress in Oceanography*, 83, 1–14. https://doi.org/10.1016/j.pocean.2009.08.001

Friederich, G. E., Ledesma, J., Ulloa, O., & Chavez, F. P. (2008). Air-sea carbon dioxide fluxes in the coastal southeastern tropical Pacific. *Progress in Oceanography*, 79(2–4), 156–166. https://doi.org/10.1016/j.pocean.2008.10.001

Frölicher, T. L., & Joos, F. (2010). Reversible and irreversible impacts of greenhouse gas emissions in multi-century projections with the NCAR global coupled carbon cycle-climate model. *Climate Dynamics*, 35, 1439–1459. https://doi.org/10.1007/s00382-009-0727-0

Frölicher, T. L., Rodgers, K. B., Stock, C. A., & Cheung, W. W. L. (2016). Sources of uncertainties in 21st century projections of potential ocean ecosystem stressors. *Global Biogeochemical Cycles*, 30, 1224–1243. https://doi.org/10.1002/2015GB005338

Garcia, H. E., Boyer, T. P., Locarnini, R. A., Antonov, J. I., Mishonov, A. V., Baranova, O. K., et al. (2014a). World Ocean Atlas 2013, volume 3: Dissolved oxygen, apparent oxygen utilization, and oxygen saturation. In *NOAA Atlas NESDIS* (Vol. 75, 27 pp.). Washington, DC: National Oceanic and Atmospheric Administration.

Garcia, H. E., Locarnini, R. A., Boyer, T. P., Antonov, J. I., Baranova, O. K., Zweng, M. M., et al. (2014b). World Ocean Atlas 2013, volume 4: Dissolved inorganic nutrients (phosphate, nitrate, silicate). In *NOAA Atlas NESDIS* (Vol. 76, 25 pp.). Washington, DC: National Oceanic and Atmospheric Administration. https://doi.org/10.1182/blood-2011-06-357442

Gattuso, J.-P., Magnan, A., Bille, R., Cheung, W. W. L., Howes, E. L., Joos, F., et al. (2015). Contrasting futures for ocean and society from different anthropogenic CO_2 emissions scenarios. *Science*, *349*(6243), aac4722. https://doi.org/10.1126/science.aac4722

Graven, H., Gruber, N., Key, R., Khatiwala, S., & Giraud, X. (2012). Changing controls on oceanic radiocarbon: New insights on shallow-to-deep ocean exchange and anthropogenic CO_2 uptake. *Journal of Geophysical Research*, *117*, C10005. https://doi.org/10.1029/2012JC008074

Gruber, N. (2011). Warming up, turning sour, losing breath: Ocean biogeochemistry under global change. *Philosophical Transactions of the Royal Society A*, *369*, 1980–1996. https://doi.org/10.1098/rsta.2011.0003

Gruber, N., Frenzel, H., Doney, S. C., Marchesiello, P., McWilliams, J. C., Moisan, J. R., et al. (2006). Eddy-resolving simulation of plankton ecosystem dynamics in the California Current System. *Deep Sea Research Part I: Oceanographic Research Papers*, *53*, 1483–1516. https://doi.org/10.1016/j.dsr.2006.06.005

Gruber, N., Hauri, C., Lachkar, Z., Loher, D., Frölicher, T. L., & Plattner, G.-K. (2012). Rapid progression of ocean acidification in the California Current System. *Science*, *337*, 220–223. https://doi.org/10.1126/science.1216773

Harris, K. E., DeGrandpre, M. D., & Hales, B. (2013). Aragonite saturation state dynamics in a coastal upwelling zone. *Geophysical Research Letters*, *40*, 2720–2725. https://doi.org/10.1002/grl.50460

Hauri, C., Gruber, N., Plattner, G.-K., Alin, S., Feely, R. A., Hales, B., et al. (2009). Ocean acidification in the California Current System. *Oceanography*, *22*(4), 60–71.

Hauri, C., Gruber, N., Vogt, M., Doney, S. C., Feely, R. A., Lachkar, Z., et al. (2013). Spatiotemporal variability and long-term trends of ocean acidification in the California Current System. *Biogeosciences*, *10*(1), 193–216. https://doi.org/10.5194/bg-10-193-2013

Iglesias-Rodriguez, M. D., Halloran, P. R., Rickaby, R. E. M., Hall, I. R., Colmenero-Hidalgo, E., Gittins, J. R., et al. (2008). Phytoplankton calcification in a high-CO_2 world. *Science*, *320*(5874), 336–340. https://doi.org/10.1126/science.1154122

Jiang, L-Q., Feely, R. A., Carter, B. R., Greeley, D. J., Gledhill, D. K., & Arzayus, K. M. (2015). Climatological distribution of aragonite saturation state in the global oceans. *Global Biogeochemical Cycles*, *29*, 1656–1673. https://doi.org/10.1002/2015GB005198

Joos, F., Frölicher, T., Steinacher, L. M., & Plattner, G.-K. (2011). Impact of climate change mitigation on ocean acidification projections. In J.-P. Gattuso & L. Hansson (Eds.), *Ocean acidification* (chap. 14, pp. 272–290). Oxford, UK: Oxford University Press.

Key, R. M., Kozyr, A., Sabine, C. L., Lee, K., Wanninkhof, R., Bullister, J. L., et al. (2004). A global ocean carbon climatology: Results from Global Data Analysis Project (GLODAP). *Global Biogeochemical Cycles*, *18*, GB4031. https://doi.org/10.1029/2004GB002247

Kroeker, K. J., Kordas, R. L., Crim, R., Hendriks, I. E., Ramajo, L., Singh, G. S., et al. (2013). Impacts of ocean acidification on marine organisms: Quantifying sensitivities and interaction with warming. *Global Change Biology*, *19*(6), 1884–1896. https://doi.org/10.1111/gcb.12179

Lachkar, Z. (2014). Effects of upwelling increase on ocean acidification in the California and Canary Current systems. *Geophysical Research Letters*, *41*, 90–95. https://doi.org/10.1002/2013GL058726

Lachkar, Z., & Gruber, N. (2012). A comparative study of biological production in eastern boundary upwelling systems using an artificial neural network. *Biogeosciences*, *9*(1), 293–308. https://doi.org/10.5194/bg-9-293-2012

Landschützer, P., Gruber, N., Bakker, D. C. E., & Schuster, U. (2014). Recent variability of the global ocean carbon sink. *Global Biogeochemical Cycles*, *28*, 927–949. https://doi.org/10.1002/2014GB004853

Landschützer, P., Gruber, N., Bakker, D. C. E., Schuster, U., Nakaoka, S., Payne, M. R., et al. (2013). A neural network-based estimate of the seasonal to inter-annual variability of the atlantic ocean carbon sink. *Biogeosciences*, *10*(11), 7793–7815. https://doi.org/10.5194/bg-10-7793-2013

Lauvset, S. K., Key, R. M., Olsen, A., van Heuven, S., Velo, A., Lin, X., et al. (2016). A new global interior ocean mapped climatology: The 1° × 1° GLODAP version 2. *Earth System Science Data*, *8*(2), 325–340. https://doi.org/10.5194/essd-8-325-2016

Lee, K., Tong, L. T., Millero, F. J., Sabine, C. L., Dickson, A. G., Goyet, C., et al. (2006). Global relationships of total alkalinity with salinity and temperature in surface waters of the world's oceans. *Geophysical Research Letters*, *33*, L19605. https://doi.org/10.1029/2006GL027207

Locarnini, R. A., Mishonov, A. V., Antonov, J. I., Boyer, T. P., Garcia, H. E., Baranova, O. K., et al. (2013). World Ocean Atlas 2013. Vol. 1: Temperature. In S. Levitus (Ed.) & A. Mishonov (Tech. Ed.), *NOAA Atlas NESDIS* (Vol. 73, 40 pp.). Washington, DC: National Oceanic and Atmospheric Administration. https://doi.org/10.1182/blood-2011-06-357442

Lovenduski, N. S., McKinley, G. A., Fay, A. R., Lindsay, K., & Long, M. C. (2016). Partitioning uncertainty in ocean carbon uptake projections: Internal variability, emission scenario, and model structure. *Global Biogeochemical Cycles*, *30*, 1276–1287. https://doi.org/10.1002/2016GB005426

Maas, A. E., Wishner, K. F., & Seibel, B. A. (2012). The metabolic response of pteropods to acidification reflects natural CO_2-exposure in oxygen minimum zones. *Biogeosciences*, *9*(2), 747–757. https://doi.org/10.5194/bg-9-747-2012

Mackey, K. R. M., Morris, J. J., Morel, F. M., & Kranz, S. A. (2015). Response of photosynthesis to ocean acidification. *Oceanography*, *28*(2), 74–91. https://doi.org/10.5670/oceanog.2015.33

Marchesiello, P., McWilliams, J. C., & Shchepetkin, A. F. (2003). Equilibrium structure and dynamics of the California Current System. *Journal of Physical Oceanography*, *33*, 753–783.

Mayol, E., Ruiz-Halpern, S., Duarte, C. M., Castilla, J. C., & Pelegrí, J. L. (2012). Coupled CO_2 and O_2-driven compromises to marine life in summer along the Chilean sector of the Humboldt Current System. *Biogeosciences*, *9*(3), 1183–1194. https://doi.org/10.5194/bg-9-1183-2012

McNeil, B. I., & Matear, R. J. (2008). Southern Ocean acidification: A tipping point at 450-ppm atmospheric CO_2. *Proceedings of the National Academy of Sciences of the United States of America*, *105*(48), 18860–18864. https://doi.org/10.1073/pnas.0806318105

Mehrbach, C., Culberson, C. H., Hawley, J. E., & Pytkowicz, R. M. (1973). Measurement of the apparent dissociation constants of carbonic acid in seawater at atmospheric pressure. *Limnology and Oceanography*, *18*, 897–907.

Milliman, J. D. (1993). Production and accumulation of calcium carbonate in the ocean: Budget of a nonsteady state. *Global Biogeochemical Cycles*, *7*(4), 927–957.

Obersteiner, M., Bednar, J., Wagner, F., Gasser, T., Ciais, P., & Forsell, N. (2018). How to spend a dwindling greenhouse gas budget. *Nature Climate Change*, *8*, 7–10.

Orr, J. C. (2011). Recent and future changes in ocean carbonate chemistry. In J. P. Gattuso & L. Hansson (Eds.), *Ocean acidification* (chap. 3, pp. 41–66). Oxford, UK: Oxford University Press.

Orr, J. C., Aumont, O., Bopp, L., Caldeira, K., Doney, S. C., Fabry, V. J., et al. (2005). Aragonite undersaturation in the high-latitude surface ocean within the 21st century. *Nature*, *437*, 681–686.

Pauly, D., & Christensen, V. (1995). Primary production required to sustain global fisheries. *Nature*, *374*, 255–257.

Pörtner, H.-O., Karl, D., Boyd, P., Cheung, W., Lluch-Cota, S., Nojiri, Y., et al. (2014). Ocean systems. In C. B. Field et al. (Eds.), *Climate change 2014: Impacts, adaptation, and vulnerability*. Part A: Global and sectoral aspects. Contribution of Working Group II to the fifth assessment report of the Intergovernmental Panel on Climate Change (pp. 411–484). Cambridge, UK: Cambridge University Press.

Qi, D., Chen, L., Chen, B., Gao, Z., Zhong, W., Feely, R. A., et al. (2017). Increase in acidifying water in the western Arctic Ocean. *Nature Climate Change*, *7*(3), 195–199.

Resplandy, L., Bopp, L., Orr, J. C., & Dunne, J. P. (2013). Role of mode and intermediate waters in future ocean acidification: Analysis of CMIP5 models. *Geophysical Research Letters*, *40*, 3091–3095. https://doi.org/10.1002/grl.50414

Ridgway, K. R., Dunn, J. R., & Wilkin, J. L. (2002). Ocean interpolation by four-dimensional weighted least squares-application to the waters around australasia. *Journal of Atmospheric and Oceanic Technology*, *19*(9), 1357–1375. https://doi.org/10.1175/1520-0426(2002)019<1357:OIBFDW>2.0.CO;2

Risien, C. M., & Chelton, D. B. (2008). A global climatology of surface wind and wind stress fields from eight years of QuikSCAT scatterometer data. *Journal of Physical Oceanography*, *38*(1989), 2379–2413. https://doi.org/10.1175/2008JPO3881.1

Rodgers, K. B., Lin, J., & Frölicher, T. L. (2015). Emergence of multiple ocean ecosystem drivers in a large ensemble suite with an Earth system model. *Biogeosciences*, *12*, 3301–3320. https://doi.org/10.5194/bg-12-3301-2015

Rykaczewski, R. R., & Dunne, J. P. (2010). Enhanced nutrient supply to the california current ecosystem with global warming and increased stratification in an Earth system model. *Geophysical Research Letters*, *37*, L21606. https://doi.org/10.1029/2010GL045019

Sabine, C. L., Feely, R. A., Gruber, N., Key, R. F., Lee, K., Bullister, J. L., et al. (2004). The oceanic sink for anthropogenic CO_2. *Science*, *305*, 367–371.

Sarmiento, J. L., & Gruber, N. (2006). *Ocean biogeochemical dynamics* (526 pp.). Princeton, NJ: Princeton University Press.

Shchepetkin, A. F., & McWilliams, J. C. (2005). The regional oceanic modeling system (ROMS): A split-explicit, free-surface, topography-following-coordinate oceanic model. *Ocean Modelling*, *9*(4), 347–404.

Steinacher, M., Joos, F., Frölicher, T. L., Plattner, G.-K., & Doney, S. C. (2009). Imminent ocean acidification in the arctic projected with the ncar global coupled carbon cycle-climate model. *Biogeosciences*, *6*(4), 515–533. https://doi.org/10.5194/bg-6-515-2009

Steinacher, M., Joos, F., & Stocker, T. F. (2013). Allowable carbon emissions lowered by multiple climate targets. *Nature*, *499*(7457), 197–201. https://doi.org/10.1038/nature12269

Sydeman, W. J., Garcia-Reyes, M., Schoeman, D. S., Rykaczewski, R. R., Thompson, S. A., Black, B. A., et al. (2014). Climate change and wind intensification in coastal upwelling ecosystems. *Science*, *345*(6192), 77–80. https://doi.org/10.1126/science.1251635

Takahashi, T., Sutherland, S. C., Feely, R. A., & Wanninkhof, R. (2006). Decadal change of the surface water pCO_2 in the north pacific: A synthesis of 35 years of observations. *Journal of Geophysical Research*, *111*, C07S05. https://doi.org/10.1029/2005JC003074

Takahashi, T., Sutherland, S. C., & Kozyr, A. (2013). *Global ocean surface water partial pressure of CO_2 database: Measurements performed during 1957–2012 (version 2012), Ornl/Cdiac-160, Ndp-088(V2012), 088(version 2012)*. https://doi.org/10.3334/CDIAC/OTG.NDP088(V2012)

Turi, G., Lachkar, Z., & Gruber, N. (2014). Spatiotemporal variability and drivers of pCO_2 and air-sea CO_2 fluxes in the California Current System: An eddy-resolving modeling study. *Biogeosciences*, *11*(3), 671–690. https://doi.org/10.5194/bg-11-671-2014

Turi, G., Lachkar, Z., Gruber, N., & Münnich, M. (2016). Climatic modulation of recent trends in ocean acidification in the California Current System. *Environmental Research Letters*, *11*(1), 014007. https://doi.org/10.1088/1748-9326/11/1/014007

Wang, C., Zhang, L., & Lee, S. (2014). A global perspective on CMIP5 climate model biases. *Nature Climate Change*, *4*, 201–205. https://doi.org/10.1038/nclimate2118

Zeebe, R. E., & Wolf-Gladrow, D. (2001). *CO2 in seawater: Equilibrium, kinetics, isotopes* (1st ed., 360 pp.). Amsterdam, the Netherlands: Elsevier Science.

Zweng, M. M., Reagan, J., Antonov, J., Mishonov, A., Boyer, T., Garcia, H., et al. (2013). World Ocean Atlas 2013, Volume 2: Salinity. In *NOAA Atlas NESDIS* (Vol. 74, 39 pp.). Washington, DC: National Oceanic and Atmospheric Administration. https://doi.org/10.1182/blood-2011-06-357442